



ELSEVIER

Available online at www.sciencedirect.com

SCIENCE @ DIRECT®

Nuclear Instruments and Methods in Physics Research A 526 (2004) 477–492

**NUCLEAR
INSTRUMENTS
& METHODS
IN PHYSICS
RESEARCH**
Section A

www.elsevier.com/locate/nima

Cadmium–Zinc–Telluride photon detector for epithermal neutron spectroscopy—pulse height response characterisation

M. Tardocchi^{a,b,*}, A. Pietropaolo^{c,d}, C. Andreani^{c,d}, A. Bracco^e, A. D'Angelo^{d,f},
G. Gorini^{a,b}, S. Imberti^a, R. Senesi^{c,d}, N.J. Rhodes^g, E.M. Schooneveld^g

^a *INFN, UdR Milano-Bicocca, Milano, Italy*

^b *INFN e Dipartimento di Fisica "G. Occhialini" Università degli Studi di Milano-Bicocca, Piazza Della Scienza 3, I-20126 Milano, Italy*

^c *INFN UdR Tor Vergata, Roma, Italy*

^d *Dipartimento di Fisica, Università degli Studi di Roma "Tor Vergata", Roma, Italy*

^e *Dipartimento di Fisica and INFN, Università degli Studi di Milano, Sezione di Milano, Milano, Italy*

^f *INFN, Sezione di Roma II, Roma, Italy*

^g *Rutherford Appleton Laboratory, ISIS Facility, Didcot, UK*

Received 17 November 2003; received in revised form 16 February 2004; accepted 16 February 2004

Abstract

The Resonance Detector Spectrometer was recently revised for neutron spectroscopic studies in the eV energy region. In this technique one makes use of a photon detector to record the gamma emission from analyser foils used as neutron-gamma converters. The pulse-height response of a Cadmium–Zinc–Telluride photon detector to neutron capture emission from ²³⁸U and ¹⁹⁷Au analyser foils was characterised in the neutron energy range 1–200 eV. The experiment was performed on the VESUVIO spectrometer at the ISIS neutron-pulsed source. A biparametric data acquisition, specifically developed for these measurements, allowed the simultaneous measurements of both the neutron time of flight and γ pulse-height spectra. Through the analysis of the γ pulse-height spectra the main components of the signal associated with resonant and non-resonant neutron absorption were identified. It was also shown that, in principle, energy discrimination can be used to improve the signal to background ratio of the neutron time-of-flight measurement.

© 2004 Elsevier B.V. All rights reserved.

PACS: 29.30.Hs; 29.30.Kv; 29.40.Wk; 61.12.Ex

Keywords: Neutron spectroscopy; Epithermal neutron; Resonance detector; CZT

*Corresponding author. INFN e Dipartimento di Fisica "G. Occhialini", Università degli Studi di Milano-Bicocca, Piazza Delia Scienza 3, I-20126 Milano, Italy. Tel.: +39-02-6448-2326; fax: +39-02-6448-2367.

E-mail address: marco.tardocchi@mib.infn.it (M. Tardocchi).

1. Introduction

The Resonance Detector Spectrometer (RDS) was originally proposed for neutron spectroscopic studies in condensed matter at energies in the

electronvolt (eV) range [1]. Such instrument, operating as an inverse geometry spectrometer, appeared suited for the study of medium and high-energy excitations in solids and liquids at intermediate and small momentum transfers. Since then several prototype spectrometers have been proposed for operation on pulsed neutron sources [2–5]. A common and important component of these instruments was the resonance detector, composed of a resonant foil coupled to either a scintillator or a semiconductor detector. This equipment, placed in the scattered beam, was used for selection of the energy of the scattered neutrons and for their detection [6]. The inelastic neutron scattering experiments are performed employing the Resonance Detector Technique where nuclear resonances of selected isotopes, such as ^{197}Au and ^{238}U in the form of metallic foils (analyser foils), are located in the secondary flight path. These resonance filters select the energy of the scattered neutrons in a narrow energy window. The prompt capture γ -rays (as well as X-rays), which are emitted following resonant neutron absorption, are detected by scintillator or solid-state semiconductor detectors [7–9]. The time-of-flight spectra recorded by the detectors represent the scattering signal. There were two main limitations in the RDS approach when first attempted [4]: a poor signal-to-background ratio of the measurement and the requirement for heavy shielding around the resonance detector in order to reduce the γ and neutron background contamination. For these reasons the RDS concept was soon abandoned in favour of the Resonance Filter Spectrometer (RFS) [10]. The latter configuration has indeed operated the eVS spectrometer [10] at the ISIS pulsed neutron source since the middle 1980s. Recently this instrument has been superseded by the VESUVIO [11] spectrometer, which is routinely used for deep inelastic neutron scattering (DINS) measurements [12]. The user program addresses the study of single-particle dynamics in a variety of condensed matter systems. In the RFS, one still uses the analyser foils as resonance filters but detection is realised via ^6Li -glass scintillation detectors. The scattered signal is reconstructed by the Filter Difference method [13], i.e. by performing a

difference between two measurements, the first with the filter in the scattered beam (foil in) and the second with the filter removed (foil out). Given the pulsed nature of the source, the energy of the incoming neutrons, in both RDS and RFS configurations, is determined by the time-of-flight technique. The whole kinematics of the scattering process, i.e. energy, $\hbar\omega$, and wavevector, q , transfers, can then be reconstructed [13].

With the aim of accessing an extended $(q, \hbar\omega)$ kinematical range, the RDS concept was recently reconsidered for inelastic neutron scattering measurements at eV energies on the VESUVIO spectrometer [14–17]. Ideally one would like to investigate scattering processes with detection of neutrons of final energy up to about 100–150 eV coupled with a low momentum transfer below 10 \AA^{-1} . Such requirements imply the use of γ scintillators or solid-state detectors instead of the ^6Li -glass neutron scintillators detectors. The latter has in fact an intrinsic limitation in detection efficiency for energy of the scattered neutrons above 20 eV. The RDS concept exploits (n, γ) resonance reactions which occur in specific isotopes. As in the case of the RFS configuration, the analyser foil ($^A_Z X$) strongly absorbs, over a narrow energy interval (Γ_R), those scattered neutrons with energies close to the resonance E_R . The distinction comes next. The compound nucleus ($^{A+1}_Z X$), left in an excited state, radiatively decays to the ground state generating a prompt ($t \approx 10^{-16} \text{ S}$) γ -ray cascade, which covers a wide energy spectrum, ranging from tens of keV to several MeV. The highest γ energy value depends on the value of the neutron binding energy in the specific absorbing nuclide. Coupled to the analyser foil is a γ detector which tags the final neutron energy by detecting the photon cascade. In this way the kinematics of the scattering event can be reconstructed through the time-of-flight technique.

In recent DINS experiments carried out on the VESUVIO spectrometer the effectiveness of the RDS configuration has been assessed up to final neutron energies of about 70 eV [14] and experimental efforts have been devoted to identify the best combination of analyser foil and γ detector [15]. Tests have also been carried out with a natural uranium analyser foil coupled to a NaI(Tl)

scintillator, used to reveal the γ -cascade above 800 keV [16] and with a Si diode covering a very low-energy range ($E_\gamma < 50$ keV) [18]. The most recent work with Cadmium–Zinc–Telluride (CZT) solid-state detectors has explored a photon pulse height region of 20–300 keV. Given their good signal to background ratio and efficiency, these detectors appeared as the most promising candidates for their employment in the RDS configuration.

The aim of this paper is the characterisation of the CZT pulse height response to radiative capture γ -rays from ^{238}U and ^{197}Au analyser foils. The foils were placed in the beam in order to enhance the signal intensity. The measurement was performed on the VESUVIO spectrometer in a configuration where a biparametric—neutron time of flight versus photon pulse height (energy)—acquisition system has been specifically set-up (see Section 2). The acquired biparametric data were calibrated and properly reduced as described in Section 3, in order to derive the CZT photon energy spectrum associated with the different neutron resonances. The identification of the main features of the photon energy spectra recorded by the CZT, presented in Section 4, forms the basis to evaluate the possibility of improving the signal to background ratio of the measurements via energy selection (see Section 5). Finally, results and future prospects are summarized in Section 6.

2. Experiment

2.1. The VESUVIO spectrometer

The experiment was performed at the ISIS pulsed neutron source (Rutherford Appleton Laboratory, UK), on the VESUVIO spectrometer [11]. When the instrument operates in the RFS configuration, the scattered neutrons are normally recorded by ^6Li scintillators, located in both backscattering (angular range $135^\circ < 2\theta < 168^\circ$) and forward scattering positions (angular range $32^\circ < 2\theta < 68^\circ$) [11]. In the present experiment VESUVIO was set up as a Resonance Detector Spectrometer with the aim of characterising the response of two CZT photon detectors to the

prompt γ emission following resonant neutron absorption in ^{238}U or ^{197}Au analyser foils. In order to increase counting statistics and to achieve the best signal to background ratio, the analyser foils were located at the sample position (i.e., in the incident neutron beam), at an angle of 45° with respect to the incident neutron beam, and CZT detectors were positioned at the closest possible foil-detector distance (0.30 m) and at a scattering angle $2\theta \approx 90^\circ$. Given that for most resonances the corresponding neutron absorption lengths in the foil analysers are of the order of few tens of microns, the CZTs were positioned to view the foil side facing the incident neutron beam. In this way the γ self-absorption in the foils was minimized (see Section 2.3). The detectors viewed the sample through a 2 mm thick aluminium flange, which allowed the transmission of photons of energy above 20 keV.

2.2. The CZT detectors

CZT detectors are commercially available ternary semiconductor compounds, namely $\text{Cd}_{1-x}\text{Zn}_x\text{Te}$ with x being the blending fraction of CdTe in ZnTe. The x values range between 5% and 13%, corresponding to an energy band gap of 1.53 and 1.48 eV, respectively. The main advantages of this material, over other semiconductors (Ge or Si) traditionally used for photon spectroscopy, are the high atomic number and the high value of the band gap. The latter feature allows their use at room temperature operation. Limitations of these detectors are a modest energy resolution, typically about 3–4 keV at 122 keV, and poor charge collection properties which impose constraints on the useful crystal thickness (typically a few millimetres).

In the present experiment, two CZT detectors of different thickness t ($t = 2$ mm for CZT-1 and $t = 5$ mm for CZT-2) and from different producers were used. Their main properties are summarised in Table 1. The thicker crystal has a better energy resolution coupled to a shorter rise time. The thinner crystal was located in a pure aluminium housing in order to investigate any possible background contribution from impurities which might be present in the aluminium alloy housing of

Table 1
Main characteristics of the two CZT detectors used in this experiment

	CZT-1	CZT-2
Producer	Eurorad	eV product
Housing	pure aluminum	anodized aluminum
Crystal size (mm ³)	5 × 5 × 2	5 × 5 × 5
Pulse rise time (ns)	200	35
Pulse fall time (μs)	200	700
Energy resolution (FWHM) at 122 keV (keV)	6	4
Peak/valley	2	7

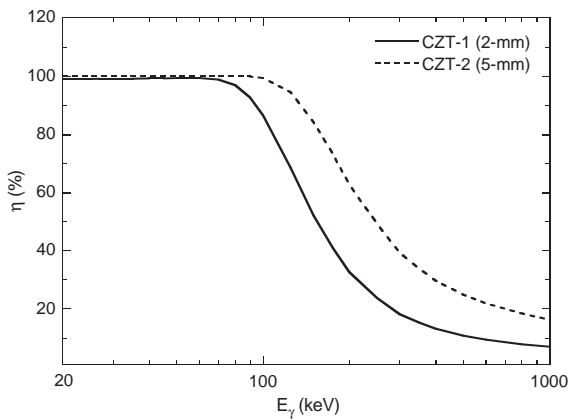


Fig. 1. Calculated photon detection efficiency (η) for the two CZT detectors used in this experiment [19]. The detector input windows set the limit for the detection of low-energy photons ($E_\gamma < 20$ keV).

the other CZT-2 detector. These detectors showed a good efficiency up to photon energies of about 200 keV. This can be appreciated in Fig. 1 where the computed efficiency [19] versus photon energy is plotted for both crystals. In the whole energy range of this figure the dominant processes for energy release in the detector are both Photoelectric and Compton interactions. At higher energies Compton interactions start to dominate and this results in incomplete energy release in the detector. The resulting spectrometer counting efficiency is therefore strongly dependent on the threshold settings of the detection electronics and is usually lower than the nominal one, i.e. about

10% for CZT-1 and 20% for CZT-2 at 1 MeV. The detectors were operated in air without any neutron or γ shielding in order to test their performance in a highly contaminated neutron and γ environment. Special care in the CZT support structure was required in order to electrically insulate the detectors and eliminate microphonic noise. The obtained result was acceptable with the exception of few cases when the detectors picked up a low pulse-height noise.

2.3. The analyser foils

In the RDS configuration the detection of the scattered neutrons results from a two-step process: (i) resonant neutron capture in the analyser foil and (ii) detection of the radiative capture γ -rays. The first process selects the mean energy of the absorbed neutrons. For a given foil thickness, the neutron absorption efficiency is determined by the resonance cross-section while the resonance width contributes to the spectrometer's instrumental resolution [20]. Thus important resonance requirements are both high cross-section (σ_R ; defined as the cross-section at the peak) and narrow width (Γ_R) [15]. The main nuclear parameters for ^{238}U and ^{197}Au resonances are summarised in the first three columns of Table 2 [21]. It can be noted that in the case of ^{238}U several high-intensity resonances are available in the energy range 1–200 eV, most of which have small values of Γ_R , varying within the energy interval 25–50 meV. In the same energy range, on the contrary, ^{197}Au has only two intense and broad resonances ($\Gamma_R > 135$ meV). As in the case of experiments employing the RFS configuration, this analyser foil in the RDS configuration appears interesting for those samples where energy-resolution requirements can be relaxed [22].

The ^{238}U and ^{197}Au analyser foils used in the present experiment had an area of 100 cm² and a thickness of 75 and 10 μm , respectively. The latter was chosen in order to ensure both good neutron absorption efficiency and low self-absorption of the radiative capture γ rays. In the case of the ^{238}U analyser foil, the neutron absorption efficiency varies from 10% for the less intense resonance ($E_n = 80.73$ eV), to nearly 100% for the most

Table 2

Main parameters (mean energy, E_R , intensity, σ_R , and width, Γ_R) of ^{238}U and ^{197}Au neutron resonances [21]

E_R (eV)	σ_R (b)	Γ_R (meV)	t_{res} (μs)
^{238}U			
6.671	23564	24.9	309.5
20.87	37966	33.7	175.0
36.68	42228	57.3	132.0
66.02	20134	48.1	98.37
80.73	2297	26.9	88.95
102.5	18989	94.4	78.94
116.9	11845	47.8	73.92
189.7	12228	197	58.03
208.5	8633	72.8	55.22
^{197}Au			
4.906	36592	139	360.9
60.3	10185	176	102.9

The right-hand column shows the calculated time-of-flight positions t_{res} of these resonances.

intense resonance ($E_n = 36.68$ eV); in this case the self-absorption probability of a 134 keV photon travelling through half of the thickness of the foil is about 19%. The ^{197}Au foil provides good neutron absorption efficiency, namely about 91% and 37% for the 4.906 and 60.3 eV resonances, respectively; the self-absorption probability of a 100 keV photon emitted from the centre of the foil is only 5%.

Energies and relative intensities of the radiative capture γ -rays following thermal neutron absorption vary for each nuclear isotope, in some cases with values of relative intensities which differ slightly [23]. The predicted γ -ray emission spectra following thermal neutron absorption in the ^{238}U and ^{197}Au isotopes, in the energy region below 700 keV, are shown in Fig. 2. One can note that the most intense γ line for ^{238}U occurs at a value of E_γ of about 12 keV and that the whole set of low-energy γ lines, i.e. 12, 48 and 134 keV, represent about 50% of the overall γ emission in the energy range of interest. In the case of ^{197}Au several intense lines are present in the region 50–300 keV and the strongest line is centred at 215 keV. Overall this isotope shows a γ emission spectrum distributed over a broader energy range compared to ^{238}U .

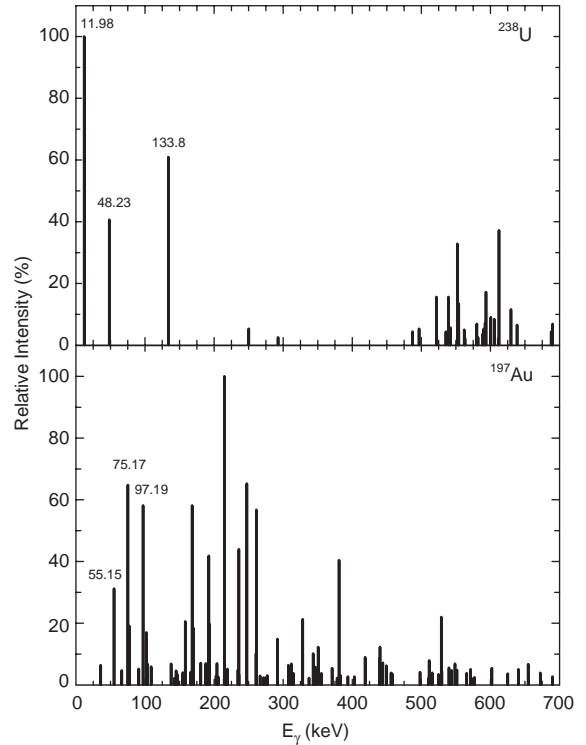


Fig. 2. Relative intensities of the radiative capture γ -rays following thermal neutron capture on ^{238}U (top) and ^{197}Au (bottom). Only the gamma lines with intensity above 2% in the shown energy region are plotted [21].

2.4. Data acquisition

A dedicated data acquisition system was developed for this experiment in the RDS set-up in order to perform simultaneous measurements of the neutron time of flight (TOF) and γ pulse height (energy) spectra. This was achieved by modifying the standard VESUVIO data acquisition electronics (DAE) which would normally record, in the RFS configuration, TOF spectra from an array of ^6Li detectors. The modified DAE recorded simultaneously both neutron TOF and photon pulse height values for each event (biparametric acquisition). Due to the limited size of the memory buffer (see below) one detector at a time could be used in biparametric data acquisition mode, while the other detector was simultaneously used in standard time of flight data acquisition mode.

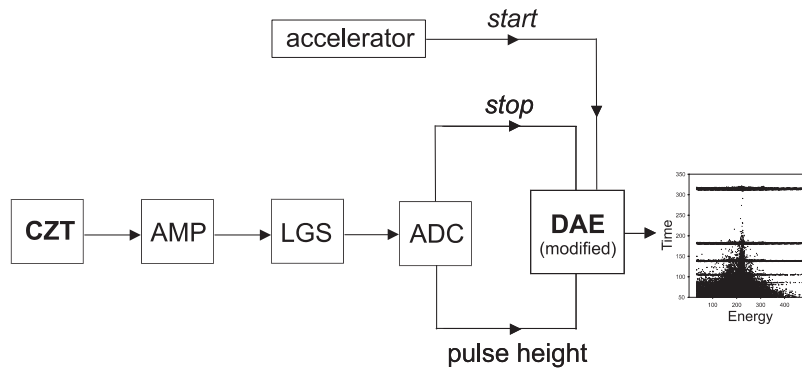


Fig. 3. Scheme of the electronic chain used for the biparametric data acquisition system which is used for the simultaneous measurement of neutron time of flight and gamma pulse height spectra from the analyzer foil. See text for details.

In the biparametric acquisition system (Fig. 3), the analog signal from the CZT was amplified and shaped by a fast Gaussian spectroscopy amplifier (AMP), with a gain of 500 and a $0.25 \mu\text{s}$ shaping time. Further signal shaping was provided by a Linear Gate & Stretcher (LGS) before sending the signal to a 12-bit Analog to Digital Converter (ADC) of the Wilkinson type with up to $12 \mu\text{s}$ variable conversion time. The digital output from the ADC was fed into the modified DAE resulting in the biparametric measurement (TOF versus Energy) sketched in Fig. 3. The ADC conversion time depends on the pulse height of the analog signal. Since the stop signal is not sent until the ADC has entirely processed the pulse, the stop signal is delayed by a time equal to the ADC conversion time. This delay can be corrected for as described in Section 3.2. The ADC has an internal lower level discriminator threshold which was set to the minimum value compatible with the noise level. Given the available memory in the DAE, the number of channels was chosen to be 512 for the TOF spectrum and 4096 for the pulse-height spectrum. This choice provided adequate time and energy resolution for the measurements.

3. Instrument calibrations and data reduction

Two different calibrations, namely energy and time calibrations, were performed for each chain of the biparametric signal processing and data

acquisition system. In this section calibration and data reduction procedures are described and illustrated with examples of data collected with both analyser foils.

3.1. Energy calibration

Absolute calibration of the pulse-height values recorded by the ADC in the biparametric data acquisition system was performed by measuring the γ spectrum from a ^{57}Co source, which provides two well-identifiable decay lines at 122 and 136 keV. An example of a ^{57}Co calibration spectrum acquired in the VESUVIO experimental hall is shown in Fig. 4 for each CZT. The two highest energy peaks, present in both pulse-height spectra, represent the ^{57}Co decay lines. The measured energy resolution at 122-keV, expressed as full-width at half-maximum (FWHM), is poorer for the CZT-1 thin detector, i.e. $\text{FWHM} = 6 \text{ keV}$, than for the CZT-2 thick one, i.e. $\text{FWHM} = 4 \text{ keV}$. It is also evident that the pulse height response of CZT-1 degrades below about 100 keV, where the spectrum shows a low peak to valley ratio and a pronounced low-energy tail. Both effects can be ascribed to an incomplete charge collection. The pulse-height spectrum of CZT-2 shows two peaks at energies below 100 keV which, due to the poorer detector response, are not visible in the CZT-1 spectrum. These peaks can be associated with characteristic *X-ray escape peaks* of Cd and Te isotopes. For instance, the peak

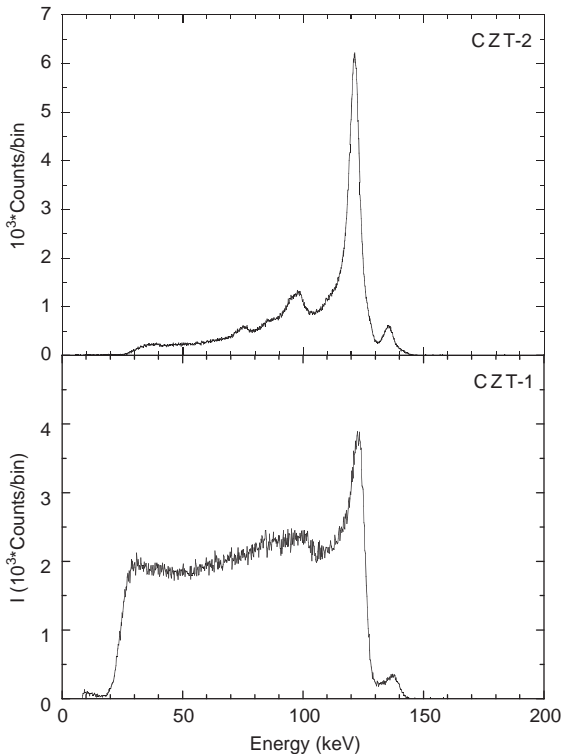


Fig. 4. Energy calibration spectra recorded with CZTs detectors from a ^{57}Co source. The energy spectra were collected in the VESUVIO experimental hall.

located at 97 keV is due to the contribution of Te ($K_{\alpha} = 27$ keV) and Cd ($K_{\alpha} = 23$ keV) X-ray photons which escape the detector. The Compton edge associated with the 122 keV full-energy peak, which is expected at 39 keV [24], is barely visible just above the ADC lower level discriminating threshold set at 30 keV. Due to its higher detector efficiency and energy resolution, only data recorded with CZT-2 have been selected for presentation in the rest of the paper.

Energy calibration measurements have been recorded routinely every few hours, in order to check the response of the CZT detectors and reveal possible radiation damage induced by fast neutrons. Due to the presence of ^{113}Cd in the lattice, which has high absorption cross-section up to a neutron energy of 400 meV, CZT detectors are expected to be sensitive to thermal neutrons. This effect has been clearly demonstrated [14]. How-

ever, the calibration measurements indicated that the CZT detectors did not show any measurable degradation of the energy resolution after about 1 month of operation at ISIS, corresponding to a fast neutron flux of about 10^{10} n cm^{-2} . Much larger fast neutron fluxes ($> 10^{12}$ n cm^{-2}) are known to be required to provide significant deterioration of the detector response [25].

3.2. Data reduction

The biparametric data presented in this paper refer to two runs acquired with the CZT-2 detector for 10 h (^{238}U) and 16 h (^{197}Au) at an average proton beam current of 180 μA . In order to obtain a suitable lineshape sampling of the time-of-flight spectrum around the time positions of the different nuclear resonances, the time binning of the modified DAE has been set with two different configurations. In the case of ^{238}U , data were collected with a 1 μs constant time bin to match the narrow intrinsic widths of the different resonances listed in Table 2. In the case of ^{197}Au broader resonances are expected and a 5 μs constant time bin was chosen. In both cases data in the time of flight region above 500 μs were recorded with a variable time binning. Pulse-height spectra were collected with the full ADC scale available (4096 channels) and constant bin size equal to 52 and 43 eV, for ^{238}U and ^{197}Au , respectively.

In the data acquisition system the stop signal is measured with an unknown delay caused by the electronic signal processing. In the case of the biparametric data acquisition system, the main contribution to such a delay comes from the ADC conversion time, t_{ADC} . The latter is written as a sum of two main contributions, i.e. $t_{\text{ADC}} = t + t(E_{\gamma})$, where t' has a constant value of about 12 μs while $t(E_{\gamma})$ is a term dependent on the energy E_{γ} deposited in the detector by the detected photon. The term $t(E_{\gamma})$ introduces a linear distortion in the data (see below) which needs to be corrected for. The constant term t' will be accounted for in the next section.

A typical *raw biparametric* spectrum relative to the ^{238}U analyser is shown in Fig. 5a. This figure represents a contour plot of signal intensity versus

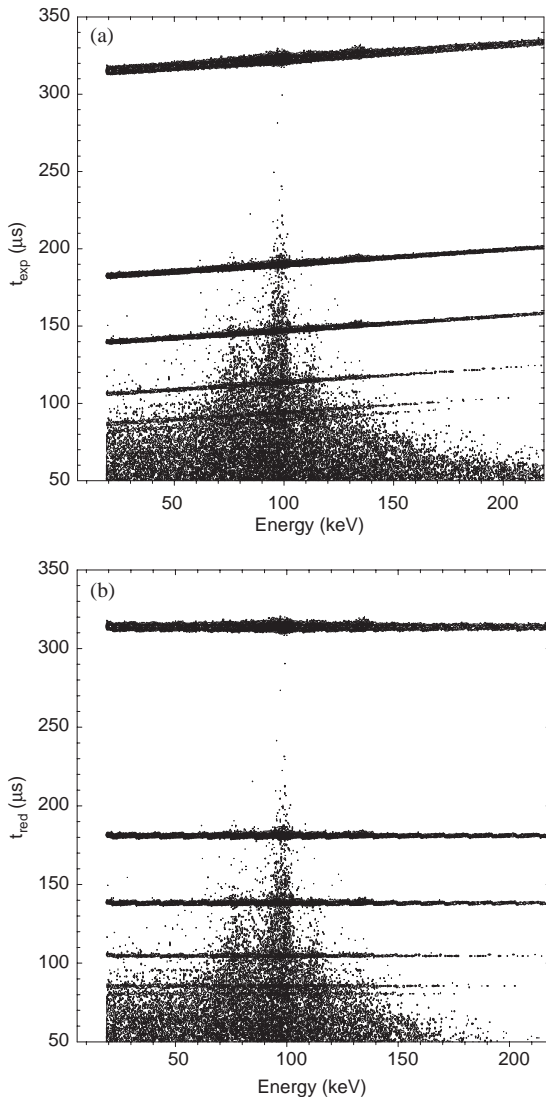


Fig. 5. Example of raw (a) and reduced (b) biparametric data by ^{238}U analyzer foil recorded with CZT-2 detector. The curves represent contour plots of spectral intensity from 10 to 200 counts in steps of 5, plotted versus neutron time-of-flight and photon energy.

γ energy (X -axis) and neutron time-of-flight, t_{exp} (Y -axis). The measured γ energies have been rebinned to 512 channels so that the effective bin size is 0.418 keV, while the spectral intensity is drawn from a threshold value of ten counts in steps of five. The horizontal stripes, occurring at a well-defined t_{exp} values, correspond to ^{238}U

resonances; for instance the stripe above $300 \mu\text{s}$ corresponds to the 6.67 eV resonance (Table 2). Besides the mentioned neutron resonances, there is an intensity distribution corresponding to a broad range of neutron time-of-flights and γ energies. This feature is related to the γ energy spectrum associated with the radiative capture of non-resonant neutrons, which arrive at all times. The stripes are tilted due to the dependence of the ADC conversion time on the γ energy, i.e. via $t(E_\gamma)$, as outlined above. As a whole such an ADC effect gives a spread of about $20 \mu\text{s}$ over the covered γ energy range. The slope of the tilted stripes ($9.33 \times 10^{-2} \mu\text{s}/\text{keV}$) is the same for all neutron resonances and the measured t_{exp} values can be corrected to obtain reduced data, t_{red} , defined by the relation $t_{\text{red}} = t_{\text{exp}} - t(E_\gamma)$. The result obtained (Fig. 5b) has an accuracy better than or equal to one time bin ($1 \mu\text{s}$) which is adequate for the purpose of this paper.

The corresponding raw and reduced data collected with the ^{197}Au analyzer foil are shown in Figs. 6a and b; here γ energy data have been rebinned to a total of 512 channels (0.345 keV), while the contour graphs are plotted from a threshold of 50 in steps of 50. In this case, the effect of the stripes' tilting is much less evident due to the coarser time bin used ($5 \mu\text{s}$). The two visible horizontal stripes correspond to the 4.906 and 60.3 eV neutron resonances (Table 2). Once the level curves in the contour plot are fixed, the time width of the stripes not only depends on the intrinsic resonance energy width, but also on the non-linear relationship between neutron time-of-flight and neutron energy ($t_{\text{res}} \propto E_{\text{res}}^{-1/2}$, see Eq. (1) in Section 3.3). Thus the same bin width, Δt , at different neutron energies corresponds to a different energy width, ΔE . In particular, there is an effective shrinking of the neutron resonances towards lower time-of-flight (higher neutron energies). This effect is particularly evident in Fig. 6b if one considers that the two resonances have comparable intrinsic widths.

3.3. Time calibration

In this section we describe how the time axis of the reduced biparametric spectrum has been

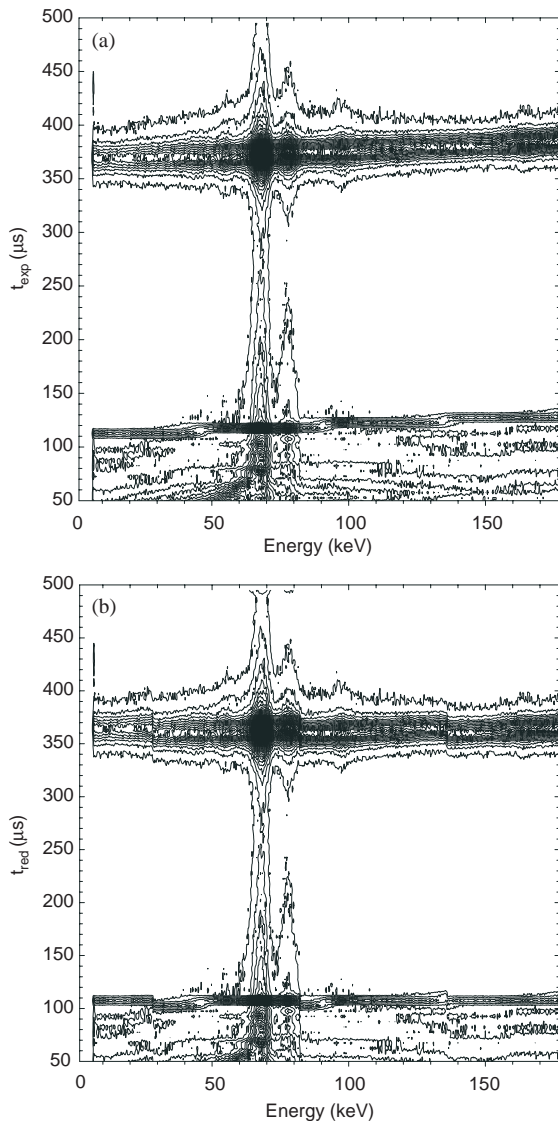


Fig. 6. Example of raw (a) and reduced (b) biparametric data by ^{197}Au analyzer foil recorded with CZT-2 detector. The curves represent contour plots of spectral intensity from 50 to 5600 counts in steps of 50, plotted versus neutron time-of-flight and photon energy.

calibrated. In an ideal acquisition, the measured neutron time of flight represents the difference $t_{\text{stop}} - t_{\text{start}}$, where t_{stop} and t_{start} are the stop and start signals of the neutron provided by the γ detector and spallation source, respectively. The time-of-flight, t_{res} , of a neutron with energy E_{res}

can be precisely calculated from the relation

$$t_{\text{res}} = \frac{L_0}{v_{\text{res}}} \quad (1)$$

where L_0 is the primary neutron flight path (distance from the moderator to the analyser foil) and v_{res} the velocity of the neutron with kinetic energy equal to the resonance energy, E_{res} . Since in the RDS configuration it is the photon which is detected, one should add the term L_1/c on the right-hand side of Eq. (1), representing the photon times-of-flight in the secondary path L_1 (analyser foil-detector distance). However, such a term, which is of the order of 1 ns, can be neglected if compared to typical values for t_{res} which are of the order of tens to hundreds of microseconds for neutron resonances in the 1–200 eV range. The calculated t_{res} values are shown in the last column of Table 2. In the real acquisition, the measured reduced data t_{red} need to be calibrated against the calculated t_{res} described below.

In this experiment the start signal is provided by the spallation source with a fixed time delay, t_{delay} ; the stop signal is also measured with a time delay, t_{ADC} , discussed in Section 3.2. The *reduced measured* time-of-flight values, t_{red} , can thus be expressed as

$$t_{\text{red}} = t_{\text{stop}} - t_{\text{star}} + t_0 \quad (2)$$

where t_0 is an offset value equal to $t' - t_{\text{delay}}$. The time calibration procedure thus consists of determining the best value of t_0 , as described below.

From the reduced biparametric spectrum one can introduce a selection window on the X -axis (energy axis) of Fig. 5b and project the data along the Y -axis (time axis). The spectrum obtained is the neutron TOF spectrum corresponding to the selected γ energy window. This is shown, for instance, in Fig. 7 for the ^{238}U reduced data; here the spectrum was produced without any energy selection, i.e. accepting photons of all energies on the X -axis of Fig. 5b above the discrimination value, set to 20 keV. Different neutron time-of-flights, shown on the X -axis of Fig. 7 with 1 μs time binning, correspond to different incident neutron energies. Nine peaks can be identified corresponding to the observable ^{238}U resonances. The intensity was normalised to the integrated

proton beam current (expressed in $\mu\text{A h}$). The time was corrected for the offset value, t_0 , as determined by fitting the measured positions in time of each resonance (t_{red} of Eq. (2)) to the calculated values (t_{res} of Eq. (1)), indicated with dashed lines in Fig. 7. This calibration procedure yields an average value of $t_0 = 6.1 \pm 0.1 \mu\text{s}$. This gives good agreement between the calculated and measured position for all the observed resonances. A similar analysis performed on ^{197}Au data yielded the TOF spectrum of Fig. 8. The data were obtained by integrating over the full γ energy range above a threshold value of 7 keV. The two peaks, corresponding to the resonances located at 4.906 and 60.3 eV, allowed the determination of $t_0 = 9 \pm 1 \mu\text{s}$.

4. Data analysis

Information that can be extracted from the collected biparametric data is dual: by introducing a selection window on the time (γ energy) axis and projecting the data along the other axis one obtains the γ energy (neutron TOF) spectrum corresponding to the selected neutron TOF (γ energy) window. This has been used for data analysis with a two-fold aim. The first aim is to characterise the CZT pulse-height response to the absorption of resonant and non-resonant neutrons in the analyser foils. The second aim is to show that it is possible to improve the signal to background ratio of the TOF measurement by selecting specific γ energy regions.

Examples of ^{238}U and ^{197}Au neutron TOF spectra obtained without any selection on the gamma energies have been shown in Figs. 7 and 8, respectively. The relative intensities of the measured neutron resonances are proportional to $I_0(E_R) w(E_R)$, where I_0 is the intensity of the incoming neutrons of energy E_R and $w = (1 - e^{-N \sigma_R^{\text{eff}} d / \cos \phi})$ the corresponding neutron absorption probability. Here N is the analyser foil atomic density, σ_R^{eff} the effective absorption cross-section at the peak, i.e. the σ_R values of Table 2 corrected for the Doppler effect at room temperature [26], d the thickness of the foil and ϕ the angle between the neutron beam direction and the normal to the

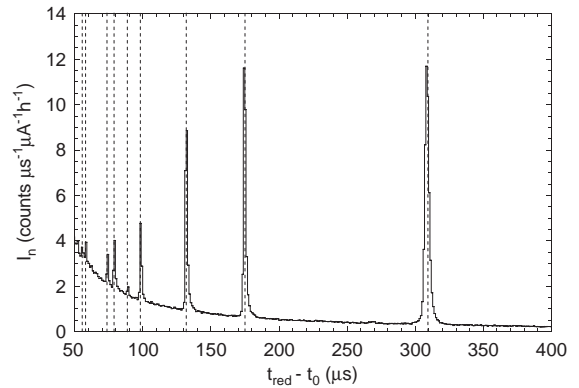


Fig. 7. Projection of ^{238}U reduced biparametric data on the time axis. The result is the neutron time-of-flight spectrum. The intensity (renormalized) is plotted versus the reduced neutron time of flight (see text). The vertical lines indicate the calculated position of the resonances; the far right peak represents the neutron resonance located at $E_n = 6.67$ eV.

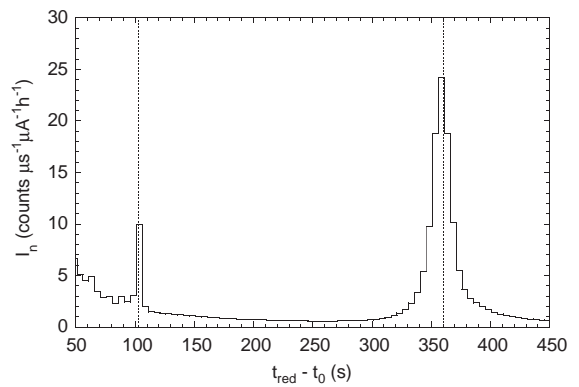


Fig. 8. Projection of ^{197}Au reduced biparametric data on the time axis. The result is the neutron time-of-flight spectrum. The vertical lines indicate the calculated positions of the resonances; the peak around 350 μs represents the $E_n = 4.906$ eV neutron resonance.

analyser foil. The line shape of each peak reflects several contributions from the analyser foil. These contributions are due to the intrinsic analyser foil cross-section with its characteristic Lorentzian shape [27], the Doppler broadening caused by the thermal lattice motion and the finite size of the thickness of the foil. In the case of ^{197}Au (Fig. 8), the peak centred at about 360 μs has wide Lorentzian wings since the main contribution to

the spectrometer's resolution comes from the intrinsic shape of the absorption cross-section. Also evident is the shrinking of the resonance as one moves towards low times-of-flight. Due to the limited memory of the DAE, the chosen time bin (5 μ s) was optimized for the 4.906 eV resonance and thus prevented any analysis of the line shape of the 60.3 eV resonance. A new faster DAE system, which will be available in future experiments, will permit bin sizes down to 0.1 μ s, necessary for a suitable line shape analysis of resonances at energies above 60 eV.

The CZT pulse-height response to neutron absorption in the foil analyser is given by the γ energy spectra associated with resonant and non-resonant neutron energy intervals. An example of such spectral analysis performed on the first four ^{238}U resonances is illustrated in Fig. 9. In each panel two spectra are shown corresponding to the resonance (continuous line) and off-resonance (dashed line) γ energy spectra. Each pair of spectra have been produced as follows. Starting from the TOF spectrum of Fig. 7, narrow time windows were selected around each neutron resonance while broad windows covered the off-resonance regions. The resonant and off-resonant γ energy spectra were thus obtained projecting the biparametric data associated with the chosen time windows along the energy axis. For instance, the pair of energy spectra of Fig. 9a were generated by selecting in Fig. 7 an 8 μ s wide time window centred around $t = 309.5 \mu$ s, i.e. the 6.671 eV resonance, and the region 193.4–293.4 μ s, i.e. an off-resonance interval. Similar time windows were chosen for the pairs of spectra associated with the resonances located $t = 175 \mu$ s ($E_n = 20.87$ eV), $t = 129 \mu$ s ($E_n = 36.68$ eV) and $t = 99 \mu$ s ($E_n = 66.02$ eV). In each panel the two spectra have been normalised to the same number of total counts, with the exception of a 16 keV wide region around the peak located at 133.8 keV.

Each pair of resonance and off-resonance spectra contain essentially the same features within statistics. Exceptions are the peak located at 133.8 keV and a slightly higher intensity in the tail at the high-energy side of the spectrum, both components being present in the on-resonance spectra only. The 133.8 keV peak is a prompt

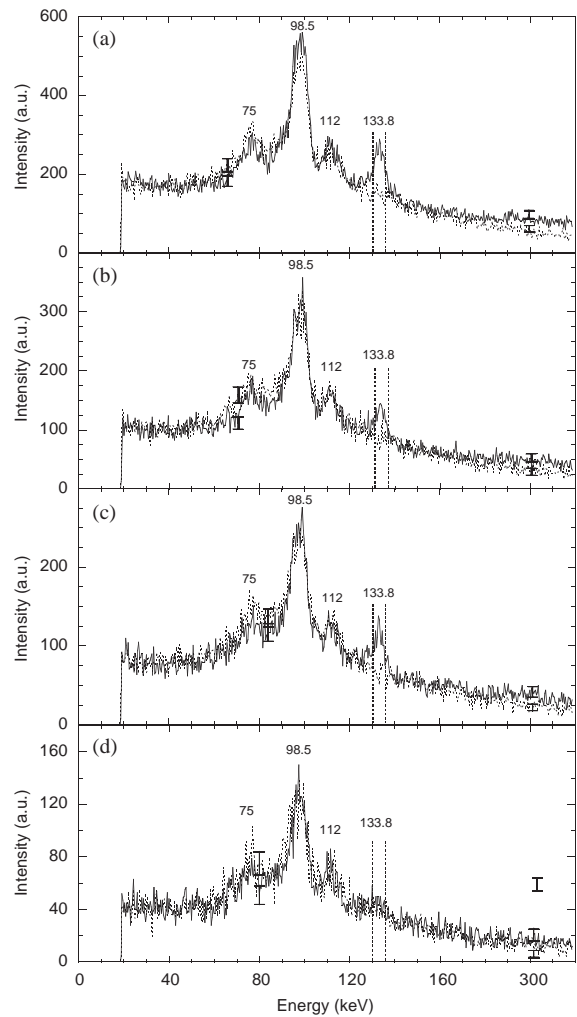


Fig. 9. Projection of ^{238}U reduced biparametric data on the energy axis for specified time intervals. The result is the γ energy spectrum from neutron capture on ^{238}U . In each panel a pair of normalised spectra (see text) is shown corresponding to a narrow time window around the neutron resonance (continuous line) and an off-resonance background region (dashed line). The chosen time intervals are: (a) $306.5 < t < 312.5 \mu$ s (resonance) and $198.5 < t < 298.5 \mu$ s (off-resonance); (b) $173.5 < t < 176.5 \mu$ s (resonance) and $138.5 < t < 168.5 \mu$ s (off-resonance); (c) $130.5 < t < 134.5 \mu$ s (resonance) and $108.5 < t < 128.5 \mu$ s (off-resonance); (d) $97.5 < t < 100.5 \mu$ s (resonance) and $90.5 < t < 96.5 \mu$ s (off-resonance). The two vertical lines select a 5 keV energy window around the γ -ray-peak at 133.8 keV. The statistical error bars are shown for illustrative purpose at the energy values of about 60–80 and 200 keV.

radiative capture γ , its broadening (4.5 keV) being entirely due to the CZT energy resolution while the tail at the high-energy side can be ascribed to Compton events induced by high-energy radiative capture γ -rays. The most intense peak, located at about 99 keV, and its neighbouring peak at 112 keV are present in both energy spectra and can be identified as K-shell X-ray lines from uranium atoms. For instance, the most prominent peak, located at 98.5 keV with a broadening of 7 keV, is due to the contribution of the 94.7 keV ($K_{\alpha 2}$) and 98.4 keV ($K_{\alpha 1}$) lines, where the latter is the most intense one [28]. These X-ray lines come from de-excitation of uranium atomic levels induced by absorption of both resonant and non-resonant neutrons; the most likely generating mechanism is believed to be internal conversion of the radiative capture γ -rays in the ^{238}U converter itself. The peak located at approximately 75 keV can be ascribed to the decay of the ^{239}U nuclei which are continuously formed via $^{238}\text{U}(n, \gamma)^{239}\text{U}$. The isotope ^{239}U decays via β^- with a half-life of about 24 min into an excited state of ^{239}Np which, in turn, radiatively decays to the ground-state emitting the most intense line at 74.7 keV. Such a line is therefore not directly associated with X-ray or prompt γ emission following neutron absorption and must be included in the background.

Similarly, selecting narrow time windows in Fig. 8 around the ^{197}Au resonances and wider off-resonance intervals, the energy spectra of Fig. 10 are obtained. The energy spectra, after normalisation to the same number of counts in the energy region 10–50 keV, show similar features to those observed for ^{238}U resonances. The most intense peaks, located at 69.0 and 78 keV, can be ascribed to K_{α} and K_{β} gold X-ray lines, respectively, while the two lower intensity peaks at 55.15 and 91.19 keV are present in the resonance spectra only. Such lines correspond to the expected γ emission for thermal neutron absorption on ^{197}Au (Fig. 2). The most intense prompt γ line emitted by ^{197}Au is at 75 keV but the low CZT energy resolution prevents its separation from the X-ray lines of Fig. 10. It can also be observed that the resonance and off-resonance normalised energy spectra differ in the high-energy part of the spectrum ($E_{\gamma} > 110$ keV). This is due to prompt

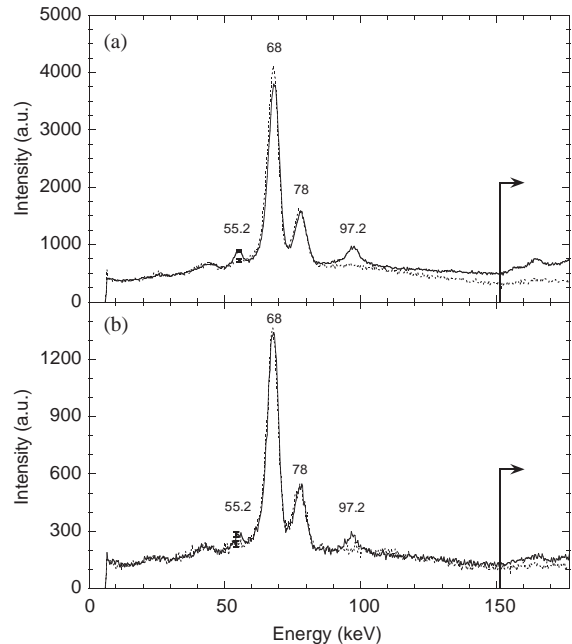


Fig. 10. Projection of ^{197}Au reduced biparametric data on the energy axis for specified time intervals. In each panel a pair of normalized spectra (see text) is shown corresponding to a narrow time window around the neutron resonance (continuous line) and an off-resonance background region (dashed line). The chosen time intervals are: (a) $343.5 < t < 373.5 \mu\text{s}$ (resonance) and $143.5 < t < 293.5 \mu\text{s}$ (off-resonance); (b) $98.5 < t < 108.5 \mu\text{s}$ (resonance) and $118.5 < t < 143.5 \mu\text{s}$ (off-resonance). The arrow on the right indicates the lower limit of a chosen energy interval. An indication of the size of the statistical errors is given for illustrative purpose at 55 keV.

high-energy photons (energy up to 6.5 MeV) emitted by ^{198}Au , which, depositing via Compton interactions a fraction of their energy in the detector, give rise to a continuous broad distribution in the energy spectrum. This feature is particularly evident in the measurements with ^{197}Au due to the presence in the radiative capture γ emission spectrum of several intense lines in the energy range 150–700 keV. For ^{238}U resonances (Fig. 9) the effect is less pronounced due to the low relative intensity of the radiative capture γ lines in the energy range above 150 keV (Fig. 2).

The measured resonance γ energy spectra have shown that the radiative prompt γ rays are indeed a clear signature of resonant neutron absorption and could be used to tag the absorption of

resonant neutrons, with the aim of improving the signal-to-background ratio (s/b) of the measurement. We have investigated such a possibility by introducing a narrow energy window ($130.5 < E_\gamma < 135.7$ keV) around the 133.8 keV γ line of ^{238}U (Fig. 9) and generating the corresponding neutron time-of-flight spectrum. The result, compared in a semi-log plot with the TOF spectrum obtained without any energy selection (Fig. 11a), indicates that a small s/b improvement can be obtained but at the price of a strong intensity reduction, as can be argued from the statistical fluctuations on the data obtained with the narrow energy window. The measured γ energy spectra of ^{197}Au seem to suggest that the best s/b can be obtained by choosing a lower level energy discrimination (LLD) at about 150 keV, as indicated in Fig. 10. The TOF spectrum obtained with this LLD threshold setting (Fig. 11b) shows

that an improvement in s/b of about 1.8 can be obtained by accepting an intensity reduction of about $\frac{1}{6}$. This shows that energy discrimination can be used as a method to improve the quality of the measurement.

5. Discussion

The measured resonance and off-resonance energy spectra of ^{238}U and ^{197}Au differ for the γ lines, thus indicating a difference in the prompt γ emission following resonant and non-resonant neutron absorption. This could be explained in terms of a significant contribution to the cross-section for off-resonance neutron absorption, given by the characteristic $1/v$ tail, from interference effects with the s- and p-wave tails of the Breit–Wigner cross-section, which describes resonance neutron absorption [29]. A comparison between the relative intensities and line shapes of the normalised γ energy spectra associated with the different resonant neutron energy intervals (Figs. 9 and 10) indicates that there are not statistically appreciable differences; the same is true for off-resonant neutron energy intervals. This seems to suggest that the radiative capture γ and X-ray emission, in the energy range accessed by this detector, is mostly independent of the absorbed neutron energy, except for the difference mentioned between resonant and non-resonant neutron absorption.

The measured energies and relative intensities of the γ lines of ^{238}U and ^{197}Au energy spectra for resonance neutron absorption are in good agreement with the database available for thermal neutron absorption. The only exception to this is the γ line at 48.2 keV which is expected in the ^{238}U emission spectrum with a relative intensity $I_\gamma = 40\%$ (Fig. 2), while the measured resonance spectra (Fig. 9) do not show any peak in that an energy range. The 133.8 keV γ line is indeed expected to be the most intense one (relative intensity $I_\gamma = 60\%$) in the energy range covered by the detector. This seems to suggest a suppression of the 48.2 keV line or at least a significant variation of its relative intensity for resonant neutron absorption as compared to thermal neutron

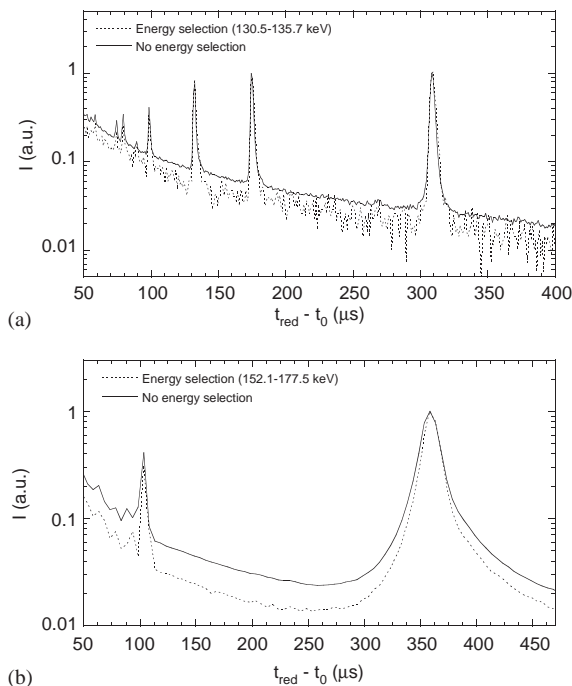


Fig. 11. Neutron time-of-flight spectra for ^{238}U (a) and ^{197}Au (b) obtained by projecting the reduced biparametric data of Fig. 5b and Fig. 6b, respectively, on the time axis for two selected γ -ray peak energy intervals. The spectra have been normalised so that the intensity of the lowest neutron energy resonance is equal to 1.

absorption. Considering the higher attenuation lengths in Al and U of a γ of 48.2 keV relative to one of 133.8 keV, the absence of the 48.2 keV line in the measured energy spectra provides an upper limit, given by the statistics, for its relative intensity of $I_\gamma < 30\%$.

The measured neutron TOF spectra (Figs. 7 and 8) have shown that s/b of these measurements is very high for many of the resonances. For instance, s/b evaluated at the resonance peak is in the range 30–40 for the two lowest-energy resonances of the uranium and gold analyser foils. Measurements have shown that nine resonances can be observed, in the data from ^{238}U , up to a neutron energy of 208.5 eV. However, the experimental set-up of the γ measurements of this paper is different from the one that is used in DINS experiments employing the RDS configuration. DINS measurements on a lead sample carried out on VESUVIO configured as RDS have shown that there is an increase of the background caused by scattered neutrons and environmental γ -rays. Data showed that neutron resonances up to 66 eV can be analyzed, whereas the background is preventing the analysis of higher energy resonances [14]. In this paper, we have shown that an improvement of s/b can be obtained by sacrificing statistics (Fig. 11). The method is most effective for ^{197}Au resonances due to a higher difference between the resonance and off-resonance energy spectra in the energy region above 150 keV. This increasing difference in the γ energy spectra at the high-energy side seems to suggest that a detector set to observe a broader energy range might have better performance. This could be a more efficient CZT or a Germanium detector. In the first case limitations are imposed by growing a thick crystal and at the same time keeping a low impurity level, while in the second case radiation damage from fast neutrons must be considered [30].

An alternative way to reduce the background is the design of a dedicated neutron and γ shield for the CZT detector. Some preliminary shielding tests have shown that the task is not trivial [31]. Special care has to be taken to absorb all moderated epithermal neutrons since the CZT detector, due to the presence of ^{113}Cd , is sensitive to thermal neutrons. Gamma shielding on the other hand,

such as lead, should have a very low content of atomic impurities (such as Sb) which have appreciable neutron resonances in the 1–100 eV region.

6. Conclusions

In this work, we have characterised the response of a Cadmium–Zinc–Telluride (CZT) solid-state detector to the radiative capture emission from ^{238}U and ^{197}Au analyser foils, which have nuclear resonances in the neutron energy range 1–100 eV. Data were acquired with an ad hoc developed biparametric data acquisition, which allowed the simultaneous measurement of the neutron time of flight and γ pulse-height spectra.

Analysis of the γ pulse-height spectra associated with resonant and non-resonant neutron absorption have shown that the observed signal is made-up of three main components: (i) X-ray emission, (ii) radiative capture γ emission and (iii) Compton continuum in the high-energy part of the spectrum. The component (i) is the most intense one and is present for both resonant and non-resonant neutron absorption, thus preventing its use for improving the signal to background ratio of the measurement via energy discrimination. The component (ii) is a clear signature of the resonant neutron absorption, but it represents only a small fraction of the overall observed signal. The component (iii), induced by radiative prompt γ -rays not fully absorbed in the detector, can contain, as in the case of ^{197}Au , a significant fraction of the overall resonance signal and could be used, in principle, for energy discrimination. We have shown that spectroscopic information, if available, could be used with an appropriate choice of energy discrimination to increase the signal-to-background ratio of the measurements, at the cost of a reduction in signal intensity. The improvement that can be obtained in the quality of the measurement depends on the sample to be studied and on the chosen analyser foil.

The measured neutron time of flight spectra have shown that neutron resonances can be measured up to neutron energies of 200 eV. This indicates that, despite the fact that the CZT signal

is dominated by prompt radiative X-ray emission induced without distinction by both resonant and non-resonant neutron absorption, the CZT detector coupled to an analyser foil can be effectively used for epithermal neutron detection. In the Resonance Detector Spectrometer (RDS) concept, the CZT is in fact used as a γ - and X-ray counter to tag resonant neutron absorption, while the neutron spectroscopic information is determined with the time-of-flight technique.

In order to extend Deep Inelastic Neutron Scattering measurements, in the RDS configuration, up to final neutron energies of 100 eV, the signal to background ratio of the measurement needs to be further improved. The present experiment seems to suggest that an improvement can be expected by detecting higher energy γ -rays, say above 150–200 keV, due to the contribution of Compton scattering events. This could be done using thicker CZT crystals, which have recently appeared on the market and have good detection efficiency up to 500 keV [32]. Alternatively a Germanium detector could be used, which however has the disadvantage of being sensitive to the radiation damage by fast neutrons [29]. In contrast, monitoring of the CZTs pulse height spectra have indicated that the detectors did not show any visible deterioration over neutron fluxes corresponding to about one month beam time.

CZTs have been shown to exhibit an excellent performance for RDS application and in addition are both robust and compact. As such these devices are good candidates for inclusion in RDS arrays providing good spatial resolution for the very low-angle detector bank, which is part of an on going upgrade of the VESUVIO spectrometer.¹

Acknowledgements

Work was performed with financial support by the European Community—Access to Research Infrastructure action of the Improving Human Potential Programme. We acknowledge Consiglio Nazionale delle Ricerche (CNR)—Italy for finan-

cial support for the experiments performed at the ISIS pulsed neutron source. One of the authors (MT) wishes to acknowledge the “Angelo Della Riccia” foundation for financial support.

References

- [1] D.R. Allen, E.W. Mitchell, R.N. Sinclair, *J. Phys. E: Sci. Instr.* 13 (1980) 639 and references quoted therein.
- [2] G.P. Felcher, J.M. Carpenter, *Nucl. Instr. and Meth.* 192 (1982) 513.
- [3] L. Cseer, N. Kroo, P. Pacher, V.G. Simlin, E.V. Vasyleva, *Nucl. Instr. and Meth.* 179 (1981) 515.
- [4] N. Watanabe, IAEA 1985 Conference Proceedings, p. 279.
- [5] J.M. Carpenter, N. Watanabe, S. Ikeda, Y. Masuda, S. Sato, H. Rauh, *Physica B* 120 (1983) 126.
- [6] C.G. Windsor, *Pulsed Neutron Scattering*, Taylor & Francis Ltd., London, 1981.
- [7] R.G. Johnson, *Nucl. Instr. and Meth. A* 263 (1988) 427.
- [8] C.D. Bowman, R.G. Johnson, J. Faber Jr. (Ed.), in: AIP Conference Proceedings No. 89, *Neutron Scattering-1981*, p. 84.
- [9] H. Rauh, S. Ikeda, N. Watanabe, *Nucl. Instr. and Meth.* 224 (1984) 469.
- [10] A.L. Fielding, J. Mayers, *Nucl. Instr. and Meth. A* 480 (2002) 680.
- [11] R. Senesi, C. Andreani, Z. Bowden, D. Colognesi, E. Degiorgi, A.L. Fielding, J. Mayers, M. Nardone, J. Norris, M. Praitano, N.J. Rhodes, W.G. Stirling, J. Tomkinson, C. Uden, *Physica B* 276–278 (2000) 200.
- [12] J. Mayers, *Phys. Rev. B* 41 (1990) 41; R.T. Azuah, W.G. Stirling, M.R. Gibbs, P.E. Sokol, J. Mayers, *Physica B* 213–214 (1995) 459; C. Andreani, P. Cipriani, D. Bolognesi, E. Pace, *J. Phys.: Condens. Matter* 12 (2000) 139; R. Senesi, C. Andreani, D. Colognesi, A. Cunsolo, M. Nardone, *Phys. Rev. Lett.* 86 (20) (2001) 4584.
- [13] J. Mayers, A.C. Evans, RAL Report RAL-91-048, 1991.
- [14] C. Andreani, A. D’Angelo, G. Gorini, S. Imberti, A. Pietropaolo, N.J. Rhodes, E.M. Schooneveld, R. Senesi, M. Tardocchi, *Appl. Phys. A* 78 (2004) 903.
- [15] A. Pietropaolo, C. Andreani, A. D’Angelo, G. Gorini, S. Imberti, N. Rhodes, E. Schooneveld, R. Senesi, M. Tardocchi, *Appl. Phys. A* 74 (2002) S189.
- [16] C. Andreani, A. Pietropaolo, R. Senesi, G. Gorini, M. Tardocchi, A. Bracco, N. Rhodes, E.M. Schooneveld, *Nucl. Instr. and Meth. A* 481 (2002) 509.
- [17] A. Pietropaolo, C. Andreani, A. D’Angelo, G. Gorini, S. Imberti, N.J. Rhodes, E.M. Schooneveld, R. Senesi, M. Tardocchi, Proceedings of the 11th International Symposium on Capture Gamma-Ray Spectroscopy and Related Topics, World Scientific, Singapore, 2003, p. 555.
- [18] M. Tardocchi, et al., Development of a silicon detector for pulsed neutron scattering experiments, manuscript in progress.

¹European project financed by the European Community in the 5th program, TMR-Access to Large Scale Facility.

- [19] B. Redus, Charge Trapping in XR-100T-CZT Detectors, Amptek Application Note ANCZT1 Rev. 1, 2000 and <http://www.amptek.com/anczt1.html>.
- [20] R.J. Newport, J. Penfold, W.G. Williams, Nucl. Instr. and Meth. 223 (1984) 120.
- [21] S.F. Mughabghab, Neutron Cross Sections, Vol. 1, Part B, Academic Press, New York, 1984.
- [22] C. Andreani, D. Colognesi, E. Degiorgi, M.A. Ricci, J. Chem. Phys. 115 (2001) 11243.
- [23] National Nuclear Data Center, Brookhaven National Laboratory, <http://www.nndc.bnl.gov> and Thermal Neutron Capture Home Page, Ernest O. Lawrence Berkeley National Laboratory, <http://ie.lbl.gov/ng.html>.
- [24] G.F. Knoll, Radiation Detection and Measurement, 3rd Edition, Wiley, New York, p. 311.
- [25] A. Cavallini, et al., Nucl. Instr. and Meth. A 458 (2001) 392.
- [26] W.E. Lamb, Phys. Rev. 55 (1939) 190.
- [27] L. Landau, E. Lifshitz, in: Fisica Teorica, Vol. 3, Mir, Moscow, 1982.
- [28] J.A. Bearden, Rev. Mod. Phys. 39 (1967) 78.
- [29] G.A. Wasson, R.E. Chrien, M.R. Bhat, M.A. Lone, M. Beer, Phys. Rev. 173 (1968) 1170.
- [30] G.F. Knoll, Radiation Detection and Measurement, 3rd Edition, Wiley, New York, p. 291.
- [31] M. Tardocchi and S. Imberti, Preliminary study of the sources of background for a CdZnTe detector used on eVs-VESUVIO, Internal memo of Physics Department “G. Occhiali”, Milano-Bicocca University, Milan, Italy, 2002.
- [32] J.M. Ryan, et al., Development of CZT strip detector modules for 0.05- to 1-MeV gamma-ray imaging spectroscopy, SPIE Conference Proceedings on X-Ray Gamma-Ray Telescopes and Instruments for Astronomy, Vol. 4851, 2003, p. 885.